AIAA JOURNAL
Vol. 40, No. 2, February 2002

Technical Notes

TECHNICAL NOTES are short manuscripts describing new developments or important results of a preliminary nature. These Notes cannot exceed six manuscript pages and three figures; a page of text may be substituted for a figure and vice versa. After informal review by the editors, they may be published within a few months of the date of receipt. Style requirements are the same as for regular contributions (see inside back cover).

Shape Optimization of Transonic Compressor Blade Using Quasi-Three-Dimensional Flow Physics

J. Chung* and K. D. Lee†
University of Illinois at Urbana–Champaign, Urbana, Illinois 61801

Nomenclature

c_{loss} = loss coefficient
F = objective function
f = base function
g = constraint function
J = number of constraints
K = numbers of design variables
$\dot{m}$ = inlet mass flow rate
P_0 = total pressure
s = percent chord
T_0 = total temperature
X = design variable
Δn = geometry perturbation normal to blade section's chord line
η = adiabatic efficiency
ω_p = Jacobian of variation of adiabatic efficiency with respect to total pressure
ω_T = Jacobian of variation of adiabatic efficiency with respect to total temperature

Subscripts

e = flow variables at exit
i = flow variables at inlet

Superscripts

L = lower limit of side constraint on design variable
U = upper limit of side constraint on design variable

Introduction

THE tremendous growth in computer technology in recent years has made three-dimensional designs of compressor blades feasible.[1] The cost of such designs, however, is still considered expensive even with today's computing power because most computational-fluid-dynamics-based design methods require a large number of flow evaluations. An alternative way to design a compressor blade is to first optimize its sections at multiple span stations and then stack them up in the spanwise direction to generate a new blade.[2] The performance of this designed blade must be compared with that of the baseline blade at design inlet mass flow rate. Because inlet mass flow rate changes with a modification of blade geometry, the back pressure has to be adjusted for the designed blade until its inlet mass flow rate reaches the design inlet mass flow rate. In sectional designs, however, it is not meaningful to adjust the back pressure separately for each of the designed sections to ascertain the gain in performance; the back pressure of a three-dimensional blade cannot be arbitrarily tuned for each section because it has to satisfy the radial equilibrium condition. This implies that the change in inlet mass flow rate after the design must be kept at a minimum for each blade section. In designs with numerical optimization, an easy way to accomplish this might be to impose a constraint on the inlet mass flow rate, but the constraint restricts modifications of blade geometry at the same time, leaving little room for optimization. In the present study, the constraint is incorporated into the objective function to conserve the design space and yet achieve an effect similar to having a constraint on inlet mass flow rate. The details of this are shown in the following section, which briefly describes a design process developed for axial transonic compressor blade sections using quasi-three-dimensional flow physics. The results and discussions follow as the design method is demonstrated with NASA rotor 37 compressor blade.

Design Process and Tools

Step 1: Grid Generation of Initial Blade Section

A C-type grid is generated around an initial blade section using GRAPE,[3] developed by Sorenson and modified by Chima. The code generates field grid points as a solution to the Poisson equation, and the source terms in the Poisson equation are chosen to improve the grid quality near the outer boundaries and the wake lines behind the blade trailing edge.

Step 2: Quasi-Three-Dimensional Navier–Stokes Flow Analysis

Flow solutions are obtained using RVCQ3D,[4] a quasi-three-dimensional Navier–Stokes flow solver developed by Chima. An explicit, four-stage Runge–Kutta scheme is employed along with local time stepping and implicit residual smoothing to accelerate convergence. Wilcox's k–ω model[5] is chosen for the turbulence modeling. As boundary conditions, the total pressure, total temperature, and absolute flow angle are specified at the inlet, as well as the static pressure at the exit. The convergence criteria for flow solution are a three orders of magnitude reduction in average residual from its initial value and the convergences of inlet mass flow rate, exit total temperature, and exit total pressure up to the fourth significant digit. The radius change and thickness variation of the streamtube geometry are obtained with the Katsanis and McNally axisymmetric throughflow code.[6]

Step 3: Evaluation of Objective and Constraint Functions

In general, a constrained optimization problem is formulated as follows:

Minimize:

$$F(\boldsymbol{X}) \tag{1}$$

Subject to:

$$g_j(\boldsymbol{X}) \le 0, \qquad j = 1, J$$

$$X_k^L \le X_k \le X_k^U, \qquad k = 1, K$$

Received 17 April 2000; revision received 13 August 2001; accepted for publication 26 September 2001.

*Graduate Research Assistant, Aeronautical and Astronautical Engineering Department. Student Member AIAA.
†Professor, Aeronautical and Astronautical Engineering Department. Associate Fellow AIAA.

In this study, the adiabatic efficiency of a compressor blade section is chosen to be optimized. Thus, from the definition of adiabatic efficiency for a single rotor, two objective functions are formulated. The first is given as

$$F_1 = -\eta/(\eta)_0 = -(1 + \omega_p \Delta p_{0e} + \omega_T \Delta T_{0e}) \tag{2}$$

where

$$\Delta p_{0e} = p_{0e} - (p_{0e})_0, \qquad \Delta T_{0e} = T_{0e} - (T_{0e})_0$$

and where subscript 0 denotes the values for the initial geometry. The weighting factors ω_p and ω_T are obtained by linearizing the variational form of the adiabatic efficiency. In the second formulation, an additional term is added to Eq. (2) to take into account the effect of changes in the inlet mass flow rate due to changes in the geometry of blade sections during the optimization process. That is,

$$F_2 = -\eta/(\eta)_0 = -(1 + \omega_p \Delta p_{0e} + \omega_T \Delta T_{0e} + \omega_{\dot m} \Delta \dot m) \tag{3}$$

where the weighting factor $\omega_{\dot m}$ is estimated from the correlation between the adiabatic efficiency and the inlet mass flow rate for the initial blade section. For the initial optimization attempt, no constraints are used because they are computationally expensive and the necessity for their presence is not known beforehand. Constraints are, thus, added only when the optimization results in a degradation of some performance characteristics.

When the objective function is found to have reached its minimum, the design process is terminated. Otherwise, the design proceeds to step 4.

Step 4: Sensitivity Analysis and Numerical Optimization

The sensitivities of the objective and constraint functions for each design variable are evaluated by finite differencing. For example, the gradient of an objective function with respect to the kth design variable is found from

$$\frac{\partial F}{\partial X_k} = \frac{F(\boldsymbol{X} + \Delta X_k) - F(\boldsymbol{X})}{\Delta X_k} \tag{4}$$

The sensitivities are fed into the optimization process driven by DOT, a commercial optimization package built by VMA Engineering,[7] which determines a step size for the vector of design variables through one-dimensional search. The optimum values of design variables are obtained when the Kuhn–Tucker condition is satisfied.

Step 5: Modification of Blade Geometry and Grid Generation

The geometry of a blade section is modified by adding a linear combination of base functions in the direction normal to the chord line of the blade. The geometry perturbation is defined as

$$\Delta n = \sum_{k=1}^{K} X_k f_k(s) \tag{5}$$

The base functions used in this study were the Hicks–Henne shape functions[8] without the function specialized for the leading edge.

The grid is regenerated for a modified blade section as described in step 1 to maintain the grid quality during the design. The design process jumps back to step 2 and iterates until the design criteria are met.

Demonstrations

The design method is demonstrated with NASA rotor 37, a core compressor blade developed in the 1970s at the NASA John H. Glenn Research Center at Lewis Field. The blade sections at 70, 50, and 30% span stations were chosen as initial geometry, and the two objective functions in Eqs. (2) and (3) were employed to maximize their adiabatic efficiencies at the design operating condition. The grid for each section had 257 grid points in the streamwise direction with 177 points on blade surfaces and 33 in the blade-to-blade direction. Four design variables were located on each blade surface, at 55, 57, 59, and 61% chord on the suction surface and at 50, 55, 60, and 65% chord on the pressure surface. They were clustered near the midchord to minimize the perturbation of blade geometry near the leading- and trailing-edge regions.

All designs took 3–7 cycles to converge, consuming about 70 CPU minutes per cycle on a single processor of SGI Origin 2000 with 300-MHz clock speed. The design results are summarized in Table 1, which shows that, for all cases, the addition of the inlet mass flow rate term to F_1 significantly reduced the change in the inlet mass flow rate during the optimization. Higher gains in the efficiency were also obtained with F_2 except for the blade section at 30% span station. The design results at 30% span station indicate that, although the gain in efficiency is the greatest among the three optimized sections, it may cause an adverse effect as part of a three-dimensional blade due to the large change in inlet mass flow rate. This implies that the blade sections near the hub region may not be suitable for quasi-three-dimensional design due to the presence of strong three-dimensional effects near the hub region. Figure 1 compares the blade geometry of the initial and designed blade sections at 50% span station, which were rotated to show the changes in geometry more clearly. The inspection on the geometry of the designed blade sections and their performances indicated no additional optimization with constraints were necessary.

In all cases, the improvements in efficiency were found to come from a combination of weakened shock strength and reduction in flow separation region. Figure 2, which shows isentropic Mach number on blade surfaces at 50% span station, shows a reduction in shock strength along with a slight delay in shock impingement point on the suction surface. From velocity vector plots near the

Table 1 Optimization results

Parameter	Initial	Design with objective function 1	Change, %	Design with objective function 2	Change, %
		Blade section of rotor 37 at 70% span			
$\dot m/\dot m_{\text{initial}}$	1.00	1.00104	0.10405	0.99994	−0.00543
η	0.88939	0.89811	0.98045	0.89933	1.11762
p_{0e}/p_{0i}	2.19158	2.18223	−0.42663	2.17559	−0.72961
p_e/p_i	1.62568	1.62666	0.06028	1.62592	0.01476
c_{loss}	0.16373	0.14939	−8.75832	0.14707	−10.17529
		Blade section of rotor 37 at 50% span			
$\dot m/\dot m_{\text{initial}}$	1.00	0.99780	−0.22022	0.99999	−0.00106
η	0.88700	0.88944	0.27508	0.89361	0.74521
p_{0e}/p_{0i}	2.13531	2.12156	−0.64393	2.11788	−0.81627
p_e/p_i	1.58637	1.58464	−0.10905	1.58649	0.00756
c_{loss}	0.19177	0.18642	−2.78980	0.17852	−6.90932
		Blade section of rotor 37 at 30% span			
$\dot m/\dot m_{\text{initial}}$	1.00	1.03203	3.20281	1.02310	2.31045
η	0.85167	0.87788	3.07748	0.87121	2.29432
p_{0e}/p_{0i}	2.00279	2.02664	1.19084	2.01853	0.78590
p_e/p_i	1.50056	1.51997	1.29352	1.51697	1.09359
c_{loss}	0.27879	0.22851	−18.03508	0.24131	−13.44381

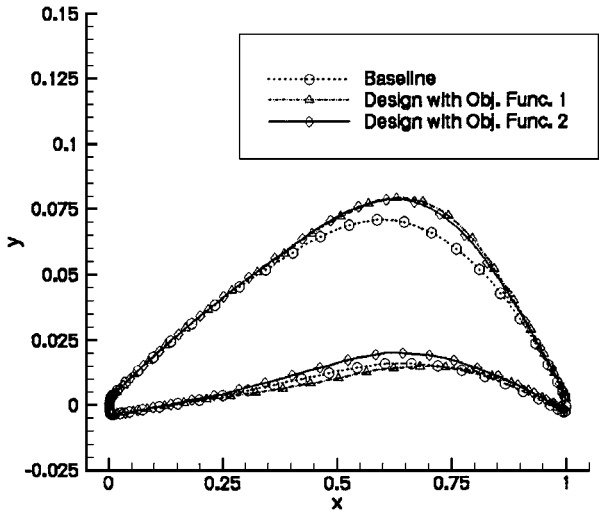

Fig. 1 Geometry of initial and designed blade sections at 50% span.

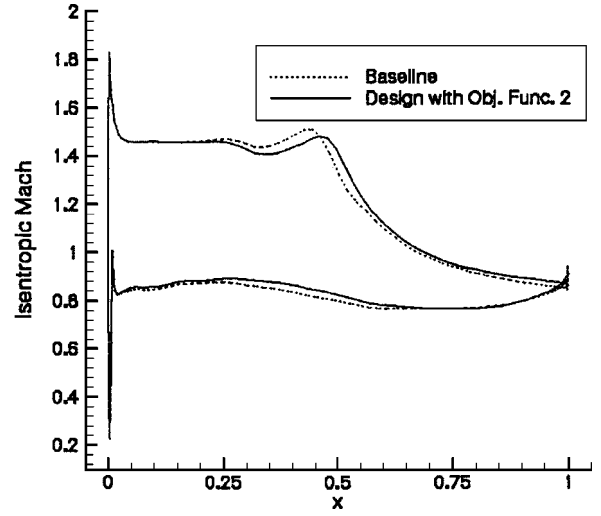

Fig. 2 Isentropic Mach numbers on blade surfaces for blade sections at 50% span.

shock impingement point, it was observed that a reduction in flow separation behind the shock ensued as a result of weakened shock strength.

Conclusions

The flowfield inside transonic compressors involves high-level flow physics and is very sensitive to changes in blade geometry. Therefore, the design of an axial compressor blade requires careful maneuvering through complex nonlinear design space. Numerical optimization is attractive in that constraints can be imposed to prevent ill effects of a design. Constraints, however, limits design space, and in the case of an axial compressor blade design, a constraint on inlet mass flow rate takes too much space away, making optimization extremely difficult to perform. This Note shows that incorporating the constraint into an objective function can improve the design results. Also if needed constraints are related to the objective function in some ways, it would be possible that they all become a part of the objective function while discouraging the design process from moving into certain directions.

The study also shows that the developed design method can improve the adiabatic efficiency of a blade section significantly by reducing the losses from the passage shock and the flow separation. The design method, however, cannot handle three-dimensional effects because it employs quasi-three-dimensional flow physics and did not produce desired design results for the blade section near the hub region. To ascertain the significance of the quasi-three-dimensional design results, constructing and evaluating the performance of three-dimensional blades based on the designed sections will be conducted in the future.

References

[1] Damle, S., Dang, T., Stringham, J., and Razinsky, E., "Practical Use of 3D Inverse Method for Compressor Blade Design," American Society of Mechanical Engineers, ASME Paper 98-GT-115, June 1998.

[2] Wang, Z., Cai, R., Chen, H., and Zhang, D., "A Fully Three-Dimensional Inverse Method for Turbomachinery Blading with Navier–Stokes Equations," American Society of Mechanical Engineers, ASME Paper 98-GT-126, June 1998.

[3] Sorenson, R. L., "A Computer Program to Generate Two-Dimensional Grids About Airfoils and Other Shapes by Use of Poisson's Equation," NASA TM-81198, 1980.

[4] Chima, R. V., "Explicit Multigrid Algorithm for Quasi-Three-Dimensional Viscous Flows in Turbomachinery," *Journal of Propulsion and Power*, Vol. 3, No. 5, 1987, pp. 397–405.

[5] Wilcox, D. C., "Comparison of Two-Equation Turbulence Models for Boundary Layers with Pressure Gradient," *AIAA Journal*, Vol. 31, No. 8, 1993, pp. 1414–1421.

[6] Katsanis, T., and McNally, W. D., "Revised FORTRAN Program for Calculating Velocities and Streamlines on the Hub-Shroud Midchannel Stream Surface of an Axial-, Radial-, and Mixed-Flow Turbomachine or Annular Duct, Part I—User's Manual," NASA TN D-8430, 1977.

[7] "DOT User's Manual," Ver. 3.00, VMA Engineering, Goleta, CA, 1992.

[8] Hicks, R. M., and Henne, P. A., "Wing Design by Numerical Optimization," *Journal of Aircraft*, Vol. 15, No. 7, 1978, pp. 407–412.

R. M. C. So
Associate Editor

Semistructured Grid Generation in Three Dimensions Using a Parabolic Marching Scheme

David S. Thompson* and Bharat K. Soni†
Mississippi State University,
Mississippi State, Mississippi 39762-9627

Introduction

STRUCTURED grids and unstructured meshes have been used successfully to solve a wide range of problems in computational mechanics.[1] Each of these mesh types has advantages and disadvantages that have been well documented in the literature. It seems apparent that meshes consisting of a single-element type cannot simultaneously address the sometimes conflicting requirements of solution accuracy, computational efficiency, and automation of the grid-generation process.

Hybrid grids[2,3] are an attempt to address these requirements by combining elements of both structured grids and unstructured meshes and are attractive because of their flexibility with respect to automation as well as feature resolution through the use of anisotropic elements. Additionally, hybrid grids require significantly fewer elements than unstructured meshes to achieve the same resolution.[2] In a typical hybrid grid, anisotropic prismatic or hexahedral cells are used in regions of the domain near boundaries dominated by large gradients in the field variables. These near-body cells are generated by extrusion of the surface mesh into the domain. Once the mesh is extruded sufficiently far into the domain, tetrahedra are employed to fill the remaining voids. If the extruded mesh

Presented as Paper 2000-1004 at the AIAA 38th Aerospace Sciences Meeting, Reno, NV, 10–13 January 2000; received 29 May 2000; revision received 30 August 2001; accepted for publication 12 October 2001.

*Associate Research Professor, Center for Computational Systems at the Engineering Research Center. Member AIAA.

†Professor of Aerospace Engineering, P.O. Box 9627, Center for Computational Systems at the Engineering Research Center. Senior Member AIAA.